

Complexity and geometry of quantum state manifolds

Zhoushen Huang¹ and Alexander V. Balatsky^{1,2,3}

¹*Institute for Materials Science, Los Alamos National Laboratory, Los Alamos, NM 87545, USA**

²*NORDITA, Roslagstullsbacken 23, SE-106 91 Stockholm, Sweden*

³*Department of Physics, University of Connecticut, Storrs, CT 06269, USA[†]*

(Dated: March 13, 2022)

We show that the Hilbert space spanned by a continuously parametrized wavefunction family—*i.e.*, a quantum state manifold—is dominated by a subspace, onto which all member states have close to unity projection weight. Its characteristic dimensionality $D_{\mathcal{P}}$ is much smaller than the full Hilbert space dimension, and is equivalent to a statistical complexity measure e^{S_2} , where S_2 is the 2nd Renyi entropy of the manifold. In the thermodynamic limit, $D_{\mathcal{P}}$ closely approximates the quantum geometric volume of the manifold under the Fubini-Study metric, revealing an intriguing connection between information and geometry. This connection persists in compact manifolds such as a twisted boundary phase, where the corresponding geometric circumference is lower bounded by a term proportional to its topological index, reminiscent of entanglement entropy.

Introduction—A ubiquitous notion in quantum physics is a state manifold, *i.e.*, a continuously parametrized wavefunction family $\Psi[\mathcal{M}] \equiv \{|\Psi(\lambda)\rangle \in \mathcal{H} | \lambda \in \mathcal{M}\}$. One example, typically encountered in the study of quantum phase transitions [1, 2], is the ground state of a Hamiltonian $H(\lambda)$, where λ may represent external field, interaction strength, adiabatic pumping, *etc.* Another one is the Hilbert space trajectory generated by time evolution, *e.g.*, after a quantum quench. Conventionally, $\Psi[\mathcal{M}]$ is analyzed through a few carefully designed characteristic quantities such as order parameters, topological indices, *etc.*, which are highly system dependent. With the recent influx of machine learning techniques [3–10], a new paradigm is emerging, where the task of identifying such reductions is delegated to domain-agnostic algorithms, and the role of human becomes instead to provide domain specific data and interpretations. In light of these developments, an important question to understand is the fundamental information limit of $\Psi[\mathcal{M}]$, namely: How much data, in principle, is enough (to enable a machine, say) to capture everything about $\Psi[\mathcal{M}]$? Standard quantum mechanics posits that everything is encoded in wavefunctions, yet their number in $\Psi[\mathcal{M}]$ is nominally infinite. A more practical formulation is thus: is there a “compression” of $\Psi[\mathcal{M}]$, from which all member wavefunctions can be efficiently reconstructed to a high fidelity?

That such a scheme should indeed exist follows from an intuitive observation: The fraction of the Hilbert space \mathcal{H} “occupied” by $\Psi[\mathcal{M}]$ must be very small. This is because in a manybody setting, the dimension of \mathcal{H} is exponentially large in system size, thus a random state in \mathcal{H} has almost zero overlap with any $|\Psi(\lambda)\rangle$, and represents a dimension that is irrelevant to $\Psi[\mathcal{M}]$. Eliminating all such dimensions brings out a much more compact subspace $\mathcal{H}_{\mathcal{P}} \subset \mathcal{H}$ which remains representative of $\Psi[\mathcal{M}]$, thereby achieving a “compression rate” $D_{\mathcal{P}}/D_{\mathcal{H}}$, where $D_{\mathcal{P}}$ is the characteristic dimensionality of $\mathcal{H}_{\mathcal{P}}$, and $D_{\mathcal{H}} = \dim(\mathcal{H})$ is the full Hilbert space dimension. We will discuss how

to identify $\mathcal{H}_{\mathcal{P}}$, and show that $D_{\mathcal{P}}$ is related to the 2nd Renyi entropy S_2 of $\Psi[\mathcal{M}]$, as well as its quantum geometric volume \mathcal{V} under the Fubini-Study metric [11],

$$D_{\mathcal{P}} = e^{S_2} \simeq \mathcal{V}/\sqrt{\pi^{d_{\mathcal{M}}}} , \quad (1)$$

where $d_{\mathcal{M}} = \dim(\mathcal{M})$ is the parameter space dimension. Toward the end we will also exemplify a topological obstruction to the trivialization of these quantities on a compact manifold. Eq. 1 reveals an intriguing connection between quantumness, information, and geometry, and is reminiscent of various aspects of the ongoing discussion regarding the nature of their mutual relations [12–18].

Principal vectors of a state manifold—To characterize the Hilbert space structure of the state manifold $\Psi[\mathcal{M}]$, it is useful to think of it as a statistical ensemble. The eigenstates of its density operator $\hat{\rho}$ then provide a basis set of \mathcal{H} which are naturally ranked by their relevance to $\Psi[\mathcal{M}]$, encoded as the eigenvalues. We briefly discuss the eigen decomposition of $\hat{\rho}$ through the *singular value decomposition* (SVD) of its amplitude matrix A . Consider an M -point uniform discretization of the parameter space $\mathcal{M} \rightarrow \{\lambda_1, \lambda_2, \dots, \lambda_M\}$. Continuum limit can be restored at the end if necessary. Taking each $|\Psi_m\rangle \equiv |\Psi(\lambda_m)\rangle$ as a $D_{\mathcal{H}}$ -dimensional column vector, the amplitude matrix A is constructed as

$$A = \frac{1}{\sqrt{M}} (|\Psi_1\rangle \ |\Psi_2\rangle \ \dots \ |\Psi_M\rangle) . \quad (2)$$

SVD of A then gives (subscripts denote matrix sizes)

$$A_{D_{\mathcal{H}} \times M} = U_{D_{\mathcal{H}} \times K} \Lambda_{K \times K} V_{K \times M}^\dagger , \quad (3)$$

in which $\Lambda_{\kappa\kappa'} = \sqrt{w_{\kappa}} \delta_{\kappa,\kappa'}$ is a positive diagonal matrix with $1 \geq w_1 \geq w_2 \geq \dots w_K > 0$, U and V are column unitary matrices, $U^\dagger U = V^\dagger V = \mathbb{I}_{K \times K}$, and $K \leq \min(D_{\mathcal{H}}, M)$ is the rank of A , which is also the *exact* dimensionality of the Hilbert space spanned by the M sampled states. In a manybody setting, $M \ll D_{\mathcal{H}}$,

thus $K = M$ if we assume all sampled states are linearly independent. The eigen decomposition of $\hat{\rho}$ then reads

$$\hat{\rho} = AA^\dagger = \frac{1}{M} \sum_{m=1}^M |\Psi_m\rangle\langle\Psi_m| = \sum_{\kappa=1}^K w_\kappa |U_\kappa\rangle\langle U_\kappa|, \quad (4)$$

where $|U_\kappa\rangle$ is the κ^{th} column of U . Note that $\text{Tr}(\hat{\rho}) = \sum_{\kappa} w_\kappa = 1$. The expansion coefficient $\langle U_\kappa | \Psi_m \rangle = (U^\dagger A)_{\kappa m} = \sqrt{M} w_\kappa V_{\kappa m}^\dagger$ only involves V and $\{w_\kappa\}$, and can be obtained alternatively via the eigen decomposition of the $M \times M$ overlap matrix G ,

$$G_{mn} \equiv \frac{1}{M} \langle \Psi_m | \Psi_n \rangle = (A^\dagger A)_{mn}, \quad G = V^\dagger \Lambda V, \quad (5)$$

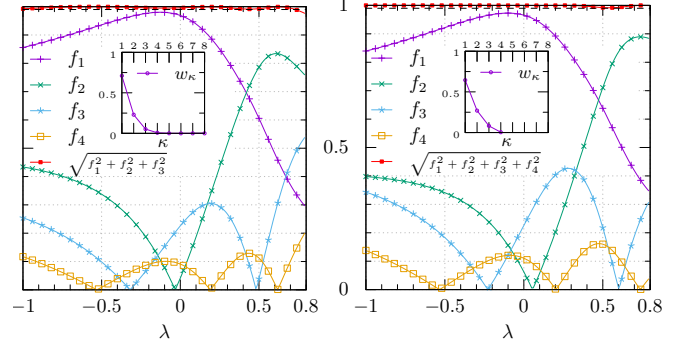
which will be useful in numerical schemes where overlaps can be efficiently computed. In statistical sciences, $\{|U_\kappa\rangle\}$ are known as *principal vectors*, and the above procedure amounts to the *principal component analysis* (PCA) of $\{|\Psi_m\rangle\}$. PCA of spin configuration data has recently been used to identify phase transitions [4, 19, 20].

We illustrate the representational power of the principal vectors using the bilinear-biquadratic $S = 1$ spin chain [21], $H(\lambda) = \sum_{x=1}^N \mathbf{S}_x \cdot \mathbf{S}_{x+1} + \lambda (\mathbf{S}_x \cdot \mathbf{S}_{x+1})^2$, where N is chain length, and $\mathbf{S}_{N+1} \equiv \mathbf{S}_1$ (periodic boundary condition). For $N = 14$, we compute its ground state (exact diagonalization) at $M = 180$ points uniformly sampled between $-1 < \lambda < 0.8$, which covers most of the gapped Haldane phase [22, 23] [24]. Their PCA, shown in Fig. 1(a), has several interesting features:

(i) The κ^{th} expansion coefficient $f_\kappa(\lambda) \equiv \langle U_\kappa | \Psi(\lambda) \rangle$ has $\kappa - 1$ nodes in the λ space. This is reminiscent of the radial nodal structure in the hydrogen atom, which is attributed to the orthogonality between states of different principal quantum numbers. A similar orthogonality exists between f_κ and $f_{\kappa'}$: $\int d\lambda f_\kappa(\lambda) f_{\kappa'}^*(\lambda) / \int d\lambda \rightarrow \frac{1}{M} \sum_{m=1}^M f_\kappa(\lambda_m) f_{\kappa'}^*(\lambda_m) = (\Lambda V^\dagger V \Lambda)_{\kappa\kappa'} = w_\kappa \delta_{\kappa,\kappa'}$, which follows from Eq. 3 [25], and is suggestive of an “emergent quantum mechanics” in the λ space.

(ii) The first few principal vectors already reproduce ~ 1 total weight. For the $N = 14$ chain, the leading weights (w_κ) are $\{0.71, 0.23, 0.052, 0.0067, \dots\}$, thus a cutoff dimension at $D_{\text{cutoff}} = 3$, for example, preserves a total weight of ~ 0.99 . Note that $D_{\text{cutoff}} \ll D_{\mathcal{H}} = 3^{14}$. Indeed, one can define a *principal Hilbert space* $\mathcal{H}_{\mathcal{P}}$ as the span of the first D_{cutoff} principal vectors; then as shown in Fig. 1(a), most ground states within the sampled region can be approximated to a fidelity of $\gtrsim 0.99$ by its projection onto $\mathcal{H}_{\mathcal{P}}$, i.e., a 3-term truncation $|\Psi(\lambda)\rangle \simeq \sum_{\kappa=1}^3 f_\kappa(\lambda) |U_\kappa\rangle$.

The compactness of $\mathcal{H}_{\mathcal{P}}$ suggests that a sparse sampling of the λ space at $M \sim D_{\text{cutoff}}$ points could gather enough information to generate as good a set of principal vectors as a dense sampling. In Fig. 1(b), we show that taking $M = 4$ samples is sufficient to approximate any *unsampled* state in the manifold. Thus the entire ground



(a) 180 evenly spaced samples (b) 4 samples at $\lambda = \pm 0.25, \pm 0.75$

FIG. 1. PCA of the bilinear-biquadratic model with 14 spins, using (a) $M = 180$ ground states evenly sampled between $-1 < \lambda < 0.8$, and (b) $M = 4$ samples at $\lambda = \pm 0.25, \pm 0.75$. $f_\kappa = |\langle U_\kappa | \Psi(\lambda) \rangle|$ are the expansion coefficients of the exact states in the principal vector basis ($1 \leq \kappa \leq M$). Insets show the first few principal weights. Note that in both cases, (i) the first three weights nearly exhaust the full weight, $w_1 + w_2 + w_3 \simeq 0.99$, and (ii) The κ^{th} expansion coefficient f_κ has $\kappa - 1$ nodes. Red squared lines show projection amplitude of the exact states onto a 3 or 4 dimensional principal Hilbert space, which almost always exceeds 0.99 (black dashed line).

state manifold can be approximately reconstructed by diagonalizing a 4×4 Hamiltonian $\tilde{H}_{\kappa\kappa'}(\lambda) = \langle U_\kappa | H(\lambda) | U_{\kappa'} \rangle$ for *continuous* λ , using $\{|U_\kappa\rangle\}$ generated from a 4-point sampling. Similarly, all physical operators are approximately 4×4 matrices.

Principal dimensionality—The impressive compactness of $\mathcal{H}_{\mathcal{P}}$ prompts the question: what determines an appropriate cutoff dimension? Below we provide an estimation. Consider a state $|\Psi_m\rangle \in \Psi[\mathcal{M}]$. Its average projection weight onto a random state in $\Psi[\mathcal{M}]$ is

$$\tilde{w}_m \equiv \frac{1}{M} \sum_{n=1}^M |\langle \Psi_m | \Psi_n \rangle|^2, \quad (6)$$

thus it takes approximately $D_m = \lceil \frac{1}{\tilde{w}_m} \rceil$ random states in $\Psi[\mathcal{M}]$ to supply a total weight of ~ 1 . In the thermodynamic limit, these D_m random states are themselves mutually orthogonal, and can serve as a minimal basis set to expand $|\Psi_m\rangle$. A further average over m removes the m -dependence, and there are two natural choices: $1/\langle \tilde{w}_m \rangle$ and $\langle 1/\tilde{w}_m \rangle$. We adopt the first one as it puts the m and n indices on an equal footing, but remark that the second option would eliminate a dominant correction ($\langle \sigma^2 \rangle$) from Eq. 13 and therefore has its own merit [26]. This leads to our definition of *principal dimensionality*,

$$D_{\mathcal{P}} \equiv \frac{1}{\langle \tilde{w}_m \rangle} = \frac{M^2}{\sum_{m,n=1}^M |\langle \Psi_m | \Psi_n \rangle|^2} = \frac{1}{\text{Tr}(G^2)}, \quad (7)$$

where $\langle \dots \rangle = \sum_m (\dots) / M \xrightarrow{M \rightarrow \infty} \int d\lambda (\dots) / \int d\lambda$.

The last equality in Eq. 7 suggests an interesting connection with Renyi entropy. Recall that the α^{th} Renyi entropy of a trace-normalized hermitian \hat{O} is $S_\alpha[\hat{O}] = \frac{1}{1-\alpha} \log \text{Tr}(\hat{O}^\alpha)$, thus $D_{\mathcal{P}} = e^{S_2[G]}$. Since $S_\alpha[\hat{O}]$ can be evaluated using the nonzero eigenvalues of \hat{O} , two operators with identical nonzero spectra—in this case $\hat{\rho} = AA^\dagger$ and $G = A^\dagger A$ —must have the same Renyi entropy, hence

$$D_{\mathcal{P}} = e^{S_2[G]} = e^{S_2[\hat{\rho}]} = \frac{1}{\sum_{\kappa=1}^K w_\kappa^2}. \quad (8)$$

Our definition of $D_{\mathcal{P}}$, based on considerations of wavefunction overlaps, is thus consistent with the intuitive correspondence between number of effective degrees of freedom and exponential of entropies [27]. The physical meaning of $D_{\mathcal{P}}$ is now more transparent: the last expression is an *inverse participation ratio*, thus $D_{\mathcal{P}}$ represents the number of principal vectors participating in the manifold $\Psi[\mathcal{M}]$, and is therefore a natural measure of its effective Hilbert space dimension, and equivalently, its degree of *Hilbert space localization* [28].

Note that $D_{\mathcal{P}}$ thus defined is not an integer. For numerical comparison, we introduce an integer truncation dimension $D(W) \equiv \min_\kappa [\sum_{\kappa'=1}^\kappa w_{\kappa'} \geq W]$, i.e., the smallest number of principal vectors needed to reach a total weight of W . We expect $D_{\mathcal{P}}$ to be comparable to a $D(W)$ with $W \sim 1$.

Since exact diagonalization of interacting models, such as the bilinear-biquadratic spin chain used earlier, can only be implemented for small system size, we now switch to a free fermion model to illustrate $D_{\mathcal{P}}$ at large N . The Su-Schrieffer-Heeger (SSH) model [29] describes fermions hopping on a one-dimensional lattice with two alternating hopping amplitudes (1 and λ) on neighboring bonds. With $2N$ lattice sites, its Hamiltonian is $H(\lambda) = \sum_{x=1}^N c_{2x-1}^\dagger c_{2x} + \lambda c_{2x}^\dagger c_{2x+1} + h.c.$, and we use periodic boundary condition $(c_{2N+1}, c_{2N+2}) = (c_1, c_2)$. Its ground state at half filling is $|\Psi(\lambda)\rangle = \prod_a \psi_{k_a}^\dagger(\lambda)|\emptyset\rangle$, where $\psi_{k_a}^\dagger(\lambda)$ creates a lower band eigenmode of momentum $k_a = 2\pi a/N$ for $a = 1, 2, \dots, N$. The weights $\{w_\kappa\}$ can be obtained by diagonalizing the overlap matrix $G_{\lambda\lambda'} = \langle\Psi(\lambda)|\Psi(\lambda')\rangle = \prod_a \langle\emptyset|\psi_{k_a}(\lambda)\psi_{k_a}^\dagger(\lambda')|\emptyset\rangle$.

In Fig. 2, we uniformly sample $M = 1000$ ground states within $-0.5 < \lambda < 0.5$, and plot $D_{\mathcal{P}}$ and $D(W)$ for several W 's, as functions of system size N . As shown, $D_{\mathcal{P}} > D(0.9)$, i.e., the first $\lceil D_{\mathcal{P}} \rceil$ principal vectors represent over 90% total weight of the state manifold. In addition, $D(W) \forall W$ are linearly related to $D_{\mathcal{P}}$ (see inset). Thus $D_{\mathcal{P}}$ accurately captures the Hilbert space size of the SSH ground state manifold.

Relation with quantum geometry—The geometric content of quantum state manifolds has been intensively studied in the past decade, particularly in relation with quantum phases and phase transitions [30–41]. Since two wavefunctions that differ by an infinitesimal $\delta\lambda$ are in general not orthogonal, their overlap ampli-

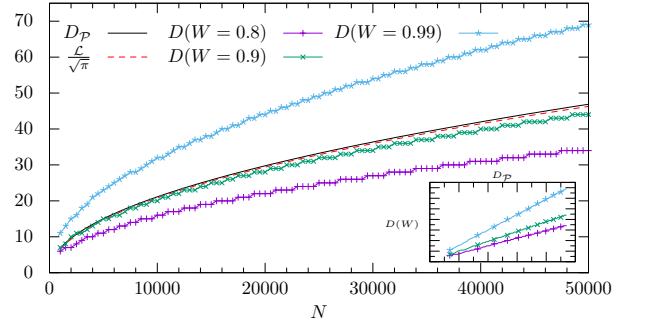


FIG. 2. Comparison of principal dimensionality $D_{\mathcal{P}}$, geometric length \mathcal{L} , and truncation dimensions $D(W)$ at different weights W , using the SSH model with $2N$ lattice sites and 1000 ground states evenly sampled between $-0.5 < \lambda < 0.5$. Note that for all N , $D_{\mathcal{P}} \simeq \frac{\mathcal{L}}{\sqrt{\pi}}$, and exceeds $D(0.9)$, i.e., the first $\lceil D_{\mathcal{P}} \rceil$ principal vectors represent $> 90\%$ total weight. Inset shows that all $D(W)$ are linearly related to $D_{\mathcal{P}}$.

tude can be interpreted as a Hilbert space distance, $d(\Psi, \Phi) = \cos^{-1} |\langle\Psi|\Phi\rangle|$, a measure of their maximal experimental distinguishability [42]. This endows $\Psi[\mathcal{M}]$ with a metric [33], $F_{\mu\nu}(\lambda) \equiv \langle\partial_{\lambda_\mu}\Psi(\lambda)|\partial_{\lambda_\nu}\Psi(\lambda)\rangle - \langle\partial_{\lambda_\mu}\Psi(\lambda)|\Psi(\lambda)\rangle\langle\Psi(\lambda)|\partial_{\lambda_\nu}\Psi(\lambda)\rangle$, which turns out to encode surprisingly rich physics. Its anti-symmetric and symmetric parts are, respectively, the Berry curvature $\Omega_{\mu\nu} = -i(F_{\mu\nu} - F_{\nu\mu})$ [43], and the Fubini-Study metric $g_{\mu\nu} = \frac{1}{2}(F_{\mu\nu} + F_{\nu\mu})$ [11]. The former has long been known to play a fundamental role in systems with non-trivial topology [43, 44]. Study of the latter in the context of quantum manybody physics initiated only more recently with Refs. [33, 35], which showed that $F_{\mu\nu}$ exhibits universal scaling near phase transitions, and becomes singular at quantum critical points. The more global aspects of $F_{\mu\nu}$ have since been systematically investigated [37, 38, 40, 41]. Note that the Fubini-Study metric can be viewed as a quantum generalization of the Fisher-Rao information metric [45], and the divergence of the latter has been shown to signify *thermal* phase transitions [46], *vis-a-vis* its quantum counterpart.

The appearance of wavefunction overlaps in Eq. 7 suggests a potential geometric interpretation of $D_{\mathcal{P}}$ and S_2 . Interestingly, Hall [47] has argued from general grounds that e^{S_1} —where S_1 is the von Neumann entropy—can be viewed as a geometric volume measure for any statistical ensemble, although Renyi entropies S_α with $\alpha \neq 0, 1$ were explicitly excluded. We now establish a connection between $D_{\mathcal{P}}$ and the Fubini-Study volume.

For clarity, we will consider a scalar parameter λ . Straightforward Taylor expansion gives $|\langle\Psi_\lambda|\Psi_{\lambda+\Delta\lambda}\rangle|^2 = 1 - g_\lambda \Delta\lambda^2 + \mathcal{O}(\Delta\lambda^3)$, where g_λ is the Fubini-Study metric,

$$g(\lambda) = \langle\partial_\lambda\Psi|\partial_\lambda\Psi\rangle - \langle\partial_\lambda\Psi|\Psi\rangle\langle\Psi|\partial_\lambda\Psi\rangle, \quad (9)$$

note that its length element reproduces the Hilbert space distance, $\delta\ell = \sqrt{g(\lambda)} \delta\lambda = \cos^{-1} |\langle\Psi_\lambda|\Psi_{\lambda+\delta\lambda}\rangle|$, and is in-

variant under reparametrization. In the thermodynamic limit, the overlap quickly drops to zero as $\Delta\lambda$ increases, thus one can write

$$|\langle\Psi(\lambda)|\Psi(\lambda+\Delta\lambda)\rangle|^2 \simeq e^{-g(\lambda)\Delta\lambda^2}. \quad (10)$$

For a parameter space $\lambda \in (\lambda_a, \lambda_b)$, this allows us to rewrite Eq. 6, in the continuum limit, as

$$\tilde{w}(\lambda) = \int_{\lambda_a}^{\lambda_b} d\lambda' \frac{e^{-g(\lambda)(\lambda'-\lambda)^2}}{\lambda_b - \lambda_a} = \sqrt{\frac{\pi}{g(\lambda)}} \frac{1 - \xi(\lambda)}{\lambda_b - \lambda_a}, \quad (11)$$

where $\xi(\lambda)$ accounts for the effect of finite integration limits, $\xi(\lambda) = \frac{1}{2}\text{erfc}[\sqrt{g(\lambda)}(\lambda - \lambda_a)] + \frac{1}{2}\text{erfc}[\sqrt{g(\lambda)}(\lambda_b - \lambda)]$, and $\text{erfc}(x) = \frac{2}{\sqrt{\pi}} \int_x^\infty dt e^{-t^2}$. $\xi(\lambda) \simeq \frac{1}{2}$ at the boundaries $\lambda_{a,b}$, but rapidly approaches zero away from them [26]. As discussed before, $\frac{1}{\tilde{w}(\lambda)}$ counts the number of random states in $\Psi[\mathcal{M}]$ needed to span $|\Psi(\lambda)\rangle$, thus away from the boundaries $\lambda_{a,b}$, \sqrt{g} is a “local density of dimensions”,

$$\sqrt{\frac{g(\lambda)}{\pi}} \simeq \frac{\tilde{w}(\lambda)^{-1}}{\lambda_b - \lambda_a} = \text{Density of principal dimension}. \quad (12)$$

One can now anticipate that the quantum geometric length $\mathcal{L} = \int d\lambda \sqrt{g(\lambda)}$, an integrated “dimension density”, should recover the principal dimensionality. Indeed, we have [26]

$$D_{\mathcal{P}} = \frac{\mathcal{L}}{\sqrt{\pi}}(1 + c) \quad , \quad \mathcal{L} \equiv \int_{\lambda_a}^{\lambda_b} d\lambda \sqrt{g(\lambda)}, \quad (13)$$

where $c = \langle \frac{1-\xi(\lambda)}{1+\sigma(\lambda)} \rangle^{-1} - 1 = \langle \xi(\lambda) \rangle - \langle \sigma(\lambda)^2 \rangle + \dots$, $\sigma(\lambda) = \frac{\sqrt{g(\lambda)}}{\langle \sqrt{g(\lambda)} \rangle} - 1$, and $\langle \dots \rangle = \frac{\int \dots d\lambda}{\int d\lambda}$. $\langle \sigma^2 \rangle$ is the relative standard deviation of \sqrt{g} independent of system size N . $\langle \xi \rangle$ is an “edge” effect around $\lambda_{a,b}$, and decreases with increasing N . Thus for a smooth enough $\Psi[\mathcal{M}]$, c should be negligible. In Fig. 2, we show that for the SSH ground state manifold, $\mathcal{L}/\sqrt{\pi}$ almost perfectly tracks $D_{\mathcal{P}}$. The Gaussian integral Eq. 11 can easily accommodate $d_{\mathcal{M}}$ -dimensional parameters, with which the dominant contribution in Eq. 13 becomes $D_{\mathcal{P}} = \mathcal{V}/\sqrt{\pi^{d_{\mathcal{M}}}}$, where $\mathcal{V} = \int d^{d_{\mathcal{M}}} \lambda \sqrt{\det(g_{\mu\nu}(\lambda))}$ is the Fubini-Study volume. Note that for gapped ground state manifolds, $g_{\mu\nu} \propto N$ where N is system size [35], thus $D_{\mathcal{P}} \propto N^{d_{\mathcal{M}}/2}$.

Compact manifold and topology—Compact manifolds may host topologically protected degeneracies, which can be interpreted as a lower bound to Hilbert space dimension. This in turn implies topological lower bounds to S_2 and \mathcal{L} . We briefly discuss this point using again the SSH model, but on the compact space of a twisted boundary phase $\theta \in [0, 2\pi]$ [48, 49], $c_{2N+i} = e^{i\theta} c_i$, $i = 1, 2$. The ground state at half filling becomes $|\Psi(\lambda, \theta)\rangle = \prod_a \psi_{k_a(\theta)}^\dagger(\lambda) |\emptyset\rangle$, where $k_a(\theta) = \frac{2\pi a + \theta}{N}$, $a = 1, 2, \dots, N$.

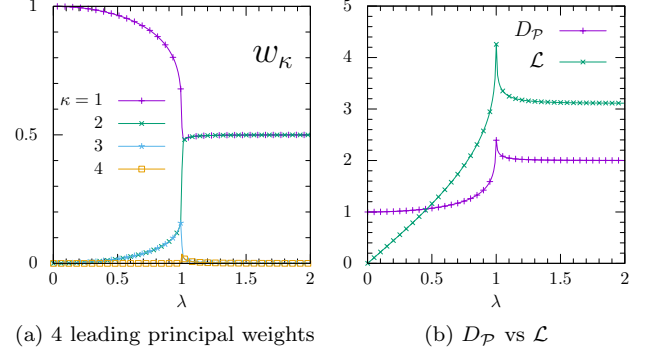


FIG. 3. SSH model with twisted boundary phase $\theta \in [0, 2\pi]$, on $2N = 400$ lattice sites. Its topological index is $|\nu| = \Theta(|\lambda| - 1)$. (a) shows the first four weights. There is one dominant weight in the non-topological phase ($\lambda < 1$), and two in the topological phase ($\lambda > 1$). (b) $D_{\mathcal{P}}$ is consistent with level counting in (a), and \mathcal{L} is lower bounded by $|\nu|\pi$, see text for discussion.

Since Bloch states with different θ are no longer orthogonal, the overlap matrix elements become Slater determinants, $G_{\theta\theta'}(\lambda) = \langle \Psi(\lambda, \theta) | \Psi(\lambda, \theta') \rangle = \det \mathcal{G}(\lambda)$, where $\mathcal{G}_{ab}(\lambda) = \langle \emptyset | \psi_{k_a(\theta)}(\lambda) \psi_{k_b(\theta')}^\dagger(\lambda) | \emptyset \rangle$. The system undergoes a topological phase transition at $|\lambda_c| = 1$, where its Berry phase $\gamma = -\int_0^{2\pi} d\theta \langle \Psi | i\partial_\theta \Psi \rangle$ changes discretely from 0 ($|\lambda| < |\lambda_c|$) to π ($|\lambda| > |\lambda_c|$).

In Fig. 3, we take a $2N = 400$ -site chain and compute $\{w_\kappa\}$, $D_{\mathcal{P}}$, and \mathcal{L} for its ground state ensemble $\{|\Psi(\theta|\lambda)\rangle\}$ at 100 θ s evenly sampled between 0 and 2π , and plot them as functions of $\lambda \in [0, 2]$. In the non-topological phase, a single weight dominates, with two degenerate subleading ones appreciating near the critical $\lambda_c = 1$; $D_{\mathcal{P}}$ stays close to 1 and only exhibits a sharp upturn near λ_c . The topological phase is dominated by two degenerate weights, thus $D_{\mathcal{P}}$ stabilizes toward 2. The cusp at λ_c reflects the topological phase transition.

The behavior of mirrors that of $D_{\mathcal{P}}$, but does not *quantitatively* satisfy $D_{\mathcal{P}} \simeq \mathcal{L}/\sqrt{\pi}$. This is expected, because the deviation of $\langle \Psi(\theta) | \Psi(\theta + \Delta\theta) \rangle$ from 1 is driven solely by the *single* bond on which the twisted boundary phase is applied, which thus spoils the many-body character of Eq. 10 and hence its quantitative accuracy. To acquire some analytical understanding, we truncate to a two-dimensional subspace, justified because $D_{\mathcal{P}} \leq 2$ in both phases except near the critical point. One can then write (dropping λ dependence) $|\Psi(\theta)\rangle = \frac{1}{\sqrt{2}} [\tilde{U}_1 + e^{i\phi(\theta)} \tilde{U}_2]$, which is the most general form of a two-component wavefunction that can host a robust winding number, $\nu = \int_0^{2\pi} \frac{d\theta}{2\pi} \partial_\theta \phi$, and $\gamma = \nu\pi$ is the Berry phase. From Eq. 9, $g(\theta) = \frac{1}{4}(\partial_\theta \phi)^2$, thus $\mathcal{L} = \frac{1}{2} \int_0^{2\pi} d\theta |\partial_\theta \phi| \geq \frac{1}{2} \left| \int_0^{2\pi} d\theta \partial_\theta \phi \right| = |\nu|\pi$. Indeed, in Fig. 3(b), \mathcal{L} stabilizes to π for $\lambda > \lambda_c$ and touches 0 at $\lambda = 0$. The geometric length of a compact manifold is

thus lower bounded by its topological index, reminiscent of the behavior of entanglement entropy [50, 51].

Conclusion and discussions—We have shown that the effective Hilbert space dimension $D_{\mathcal{P}}$ of a quantum state manifold, its complexity e^{S_2} , and its Fubini-Study geometric volume \mathcal{V} are quantitatively related, $D_{\mathcal{P}} = e^{S_2} \simeq \mathcal{V}/\sqrt{\pi^{d_{\mathcal{M}}}}$. On a compact manifold, there is a topological obstruction to their trivialization, with a lower bound determined by the topological index. The interpretation of geometric volume as a Hilbert space dimension is suggestive of an approximate “geometric quantization”, in unit of $\sqrt{\pi^{d_{\mathcal{M}}}}$, of parameter spaces (which may coincide with real space and time). This is analogous to the quantization of classical phase space in unit of $(2\pi\hbar)^d$. In this sense, $D_{\mathcal{P}}$ is a natural quantum generalization of the notion of phase space volume. For a λ that parametrizes a ground state, $D_{\mathcal{P}}$ represents the amount of quantum fluctuation driven by λ . Divergence of $g_{\mu\nu}$ at critical point [35] then implies that as one approaches quantum criticality, increasingly more states are “pulled down” from higher energies to span the effective Hilbert space. For a manifold generated from unitary time evolution (i.e., $\lambda = \text{time}$), $[D_{\mathcal{P}}]$ is roughly the number of Hilbert space dimensions “activated” over the course of time, and can be measured as the integrated energy fluctuation [52]. In the context of adiabatic quantum computation, this becomes the number of orthogonal “machine states” needed to carry out an algorithm, and is therefore a kind of computational complexity.

Acknowledgments—We are grateful to J.-X. Zhu and W. Zhu for critical reading and comments on an early draft, and to D. P. Arovas, G. Aeppli, W. Zhu, J.-X. Zhu, A. Saxena, H. Choi, T. Ahmed, and F. Ronning for various discussions. Work at LANL was supported by US DOE NNSA through LANL LDRD (XWNK). Work at NORDITA was supported by ERC DM 321031.

* zsh@lanl.gov

† avb@nordita.org

- [1] S. Sachdev, *Quantum Phase Transitions* (Cambridge University Press, 2001).
- [2] A. Dutta, G. Aeppli, B. K. Chakrabarti, U. Divakaran, T. F. Rosenbaum, and D. Sen, *Quantum phase transitions in transverse field spin models: from statistical physics to quantum information* (2010) [arXiv:1012.0653 \[cond-mat.stat-mech\]](#).
- [3] J. Carrasquilla and R. G. Melko, *Nature Physics* **13**, 431 (2017), [arXiv:1605.01735 \[cond-mat.str-el\]](#).
- [4] L. Wang, *Phys. Rev. B* **94**, 195105 (2016), [arXiv:1606.00318 \[cond-mat.stat-mech\]](#).
- [5] G. Carleo and M. Troyer, *Science* **355**, 602 (2017), [arXiv:1606.02318 \[cond-mat.dis-nn\]](#).
- [6] K. Ch’ng, J. Carrasquilla, R. G. Melko, and E. Khatami, *Physical Review X* **7**, 031038 (2017), [arXiv:1609.02552 \[cond-mat.str-el\]](#).
- [7] J. Liu, Y. Qi, Z. Y. Meng, and L. Fu, *Phys. Rev. B* **95**, 041101 (2017), [arXiv:1610.03137 \[cond-mat.str-el\]](#).
- [8] Y. Zhang and E.-A. Kim, *Physical Review Letters* **118**, 216401 (2017), [arXiv:1611.01518 \[cond-mat.str-el\]](#).
- [9] J. Chen, S. Cheng, H. Xie, L. Wang, and T. Xiang, *ArXiv e-prints* (2017), [arXiv:1701.04831 \[cond-mat.str-el\]](#).
- [10] D.-L. Deng, X. Li, and S. Das Sarma, *Physical Review X* **7**, 021021 (2017), [arXiv:1701.04844 \[cond-mat.dis-nn\]](#).
- [11] J. P. Provost and G. Vallee, *Comm. Math. Phys.* **76**, 289 (1980).
- [12] G. ’t Hooft, *ArXiv General Relativity and Quantum Cosmology e-prints* (1993), [gr-qc/9310026](#).
- [13] L. Hardy, *eprint arXiv:quant-ph/0101012* (2001).
- [14] S. Ryu and T. Takayanagi, *Physical Review Letters* **96**, 181602 (2006), [hep-th/0603001](#).
- [15] M. van Raamsdonk, *General Relativity and Gravitation* **42**, 2323 (2010), [arXiv:1005.3035 \[hep-th\]](#).
- [16] B. Swingle, *Phys. Rev. D* **86**, 065007 (2012), [arXiv:0905.1317 \[cond-mat.str-el\]](#).
- [17] X.-L. Qi, *ArXiv e-prints* (2013), [arXiv:1309.6282 \[hep-th\]](#); C. H. Lee and X.-L. Qi, *Phys. Rev. B* **93**, 035112 (2016), [arXiv:1503.08592 \[hep-th\]](#).
- [18] C. Cao, S. M. Carroll, and S. Michalakis, *Phys. Rev. D* **95**, 024031 (2017), [arXiv:1606.08444 \[hep-th\]](#).
- [19] S. J. Wetzel, *Phys. Rev. E* **96**, 022140 (2017), [arXiv:1703.02435 \[cond-mat.stat-mech\]](#).
- [20] W. Hu, R. R. P. Singh, and R. T. Scalettar, *Phys. Rev. E* **95**, 062122 (2017), [arXiv:1704.00080 \[cond-mat.stat-mech\]](#).
- [21] A. Läuchli, G. Schmid, and S. Trebst, *Phys. Rev. B* **74**, 144426 (2006), [cond-mat/0607173](#).
- [22] F. D. M. Haldane, *Phys. Rev. Lett.* **50**, 1153 (1983).
- [23] I. Affleck, T. Kennedy, E. H. Lieb, and H. Tasaki, *Phys. Rev. Lett.* **59**, 799 (1987).
- [24] We set the upper limit to 0.8 because for the finite chain length $N = 14$ used here, a premature transition to the gapless phase occurs at λ slightly above 0.8, due to finite size effect. At the thermodynamic limit $N \rightarrow \infty$, this transition should happen at $\lambda = 1$.
- [25] In fact, all $f_k(\lambda)$ are real for the bilinear-biquadratic model, which follows the real-valuedness of the Hamiltonian (and hence its ground state wavefunction). Orthogonality does not guarantee complex wavefunctions to have node(s) along the λ axis.
- [26] See Supplemental Materials for additional details.
- [27] L. D. Landau and E. M. Lifshitz, *Statistical Physics: V. 5: Course of Theoretical Physics* (Pergamon press, 1969).
- [28] D. Cohen, V. I. Yukalov, and K. Ziegler, *Phys. Rev. A* **93**, 042101 (2016), [arXiv:1511.04667 \[cond-mat.quant-gas\]](#).
- [29] W. P. Su, J. R. Schrieffer, and A. J. Heeger, *Phys. Rev. Lett.* **42**, 1698 (1979).
- [30] A. C. M. Carollo and J. K. Pachos, *Physical Review Letters* **95**, 157203 (2005), [cond-mat/0502272](#).
- [31] S.-L. Zhu, *Physical Review Letters* **96**, 077206 (2006), [cond-mat/0511565](#).
- [32] P. Zanardi and N. Paunković, *Phys. Rev. E* **74**, 031123 (2006), [quant-ph/0512249](#).
- [33] P. Zanardi, P. Giorda, and M. Cozzini, *Phys. Rev. Lett.* **99**, 100603 (2007).
- [34] W.-L. You, Y.-W. Li, and S.-J. Gu, *Phys. Rev. E* **76**, 022101 (2007), [quant-ph/0701077](#).
- [35] L. Campos Venuti and P. Zanardi, *Physical Review Let-*

- ters **99**, 095701 (2007), arXiv:0705.2211 [quant-ph].
- [36] S. Chen, L. Wang, Y. Hao, and Y. Wang, *Phys. Rev. A* **77**, 032111 (2008), arXiv:0801.0020.
- [37] S. Matsuura and S. Ryu, *Phys. Rev. B* **82**, 245113 (2010), arXiv:1007.2200 [cond-mat.mes-hall].
- [38] Y.-Q. Ma, S.-J. Gu, S. Chen, H. Fan, and W.-M. Liu, ArXiv e-prints (2012), arXiv:1202.2397 [cond-mat.str-el].
- [39] T. Neupert, C. Chamon, and C. Mudry, *Phys. Rev. B* **87**, 245103 (2013), arXiv:1303.4643 [cond-mat.str-el].
- [40] M. Kolodrubetz, V. Gritsev, and A. Polkovnikov, *Phys. Rev. B* **88**, 064304 (2013), arXiv:1305.0568 [cond-mat.stat-mech].
- [41] M. Kolodrubetz, D. Sels, P. Mehta, and A. Polkovnikov, *Phys. Rev. B* **97**, 1 (2017), arXiv:1602.01062 [cond-mat.quant-gas].
- [42] W. K. Wootters, *Phys. Rev. D* **23**, 357 (1981).
- [43] M. V. Berry, *Proceedings of the Royal Society of London A: Mathematical, Physical and Engineering Sciences* **392**, 45 (1984).
- [44] D. J. Thouless, M. Kohmoto, M. P. Nightingale, and M. den Nijs, *Phys. Rev. Lett.* **49**, 405 (1982).
- [45] S. L. Braunstein and C. M. Caves, *Phys. Rev. Lett.* **72**, 3439 (1994).
- [46] M. Prokopenko, J. T. Lizier, O. Obst, and X. R. Wang, *Phys. Rev. E* **84**, 041116 (2011).
- [47] M. J. W. Hall, *Phys. Rev. A* **59**, 2602 (1999), physics/9903045.
- [48] Q. Niu, D. J. Thouless, and Y.-S. Wu, *Phys. Rev. B* **31**, 3372 (1985).
- [49] T. Hirano, H. Katsura, and Y. Hatsugai, *Phys. Rev. B* **77**, 094431 (2008), arXiv:0710.4198 [cond-mat.str-el].
- [50] S. Ryu and Y. Hatsugai, *Phys. Rev. B* **73**, 245115 (2006), cond-mat/0601237.
- [51] P. Calabrese and J. Cardy, *Journal of Statistical Mechanics: Theory and Experiment* **6**, 06002 (2004), hep-th/0405152.
- [52] J. Anandan and Y. Aharonov, *Phys. Rev. Lett.* **65**, 1697 (1990).

SUPPLEMENTAL MATERIALS

In this note, we provide derivation details and some numerical justifications for Eq.(13) in the text, reproduced below,

$$D_{\mathcal{P}} = \frac{\mathcal{L}}{\sqrt{\pi}}(1+c) \quad , \quad \mathcal{L} = \int d\lambda \sqrt{g(\lambda)} \quad , \quad c = \left\langle \frac{1-\xi(\lambda)}{1+\sigma(\lambda)} \right\rangle^{-1} . \quad (14)$$

We also discuss an alternative definition of characteristic dimensionality, $D_{alt} \equiv \langle 1/\tilde{w}_m \rangle$ (whereas $D_{\mathcal{P}} \equiv 1/\langle \tilde{w}_m \rangle$).

Consider a one parameter wavefunction $|\Psi(\lambda)\rangle$, and discretize the λ space into a regular grid,

$$\lambda_m = m\delta\lambda \quad , \quad m = 1, 2, \dots, M \quad , \quad |\Psi_m\rangle \equiv |\Psi(\lambda_m)\rangle . \quad (15)$$

Our task is to compute $D_{\mathcal{P}}$,

$$D_{\mathcal{P}} = \sum_{m,n} \frac{M^2}{|\langle \Psi_m | \Psi_n \rangle|^2} . \quad (16)$$

We use the approximation

$$C_{mn} \equiv |\langle \Psi_m | \Psi_n \rangle|^2 \simeq \exp[-g_m(n-m)^2\delta\lambda^2] \quad , \quad (17)$$

where g_m is the Fubini-Study metric,

$$g_m \equiv g(\lambda_m) = \langle \partial_\lambda \Psi(\lambda_m) | \partial_\lambda \Psi(\lambda_m) \rangle - \langle \partial_\lambda \Psi(\lambda_m) | \Psi(\lambda_m) \rangle \langle \Psi(\lambda_m) | \partial_\lambda \Psi(\lambda_m) \rangle . \quad (18)$$

Then

$$\sum_{n=1}^M C_{mn} = \sum_{x=1-m}^{M-m} e^{-g_m x^2 \delta\lambda^2} \longrightarrow \int_{1-m}^{M-m} dx e^{-g_m x^2 \delta\lambda^2} \quad (19)$$

$$= \int_{-\infty}^{\infty} - \int_{-\infty}^{1-m} - \int_{M-m}^{\infty} \dots = \frac{\sqrt{\pi}}{\sqrt{g_m}\delta\lambda} [1 - \xi_m] \quad , \quad (20)$$

where the prefactor in the last expression results from the infinite-limit Gaussian integral, and ξ_m accounts for the second and third integration ranges on the second line, *i.e.*, the effect of finite integration limits,

$$\xi_m \equiv \xi(\lambda_m) = \frac{1}{2} \operatorname{erfc}[\sqrt{g_m}\delta\lambda(m-1)] + \frac{1}{2} \operatorname{erfc}[\sqrt{g_m}\delta\lambda(M-m)] \quad , \quad (21)$$

$$\operatorname{erfc}(x) = \frac{2}{\sqrt{\pi}} \int_x^{\infty} dt e^{-t^2} . \quad (22)$$

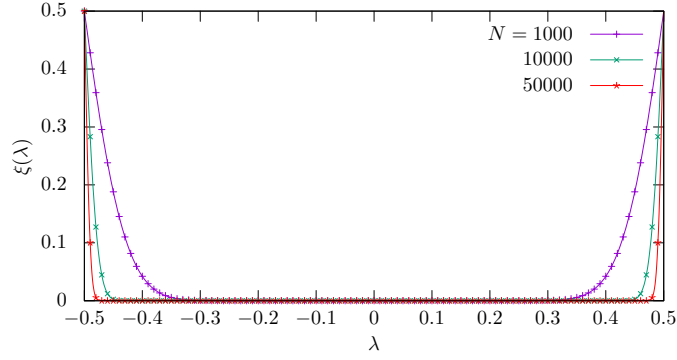


FIG. 4. ξ correction in the SSH model with periodic boundary condition. Using 1000 ground states evenly sampled between $-0.5 < \lambda < 0.5$. $\xi \sim 0.5$ close to the parameter boundaries $\lambda = \pm 0.5$, but quickly drops to zero away from them. With increasing system size N ($2N$ lattice sites), the region of non-vanishing ξ decreases.

Note that the arguments in the erfc's can be interpreted as “quantum distances” from λ_m to the two boundaries λ_1 and λ_M , respectively, as propagated by the metric at λ_m . $\xi(\lambda) \simeq \frac{1}{2}$ at the boundaries $\lambda_{a,b}$, but quickly approaches zero away from them, increasingly so with larger system size. Fig. 4 shows its behavior in the SSH model with three different system sizes.

Upon normalization, this gives the weight

$$\tilde{w}_m = \frac{1}{M} \sum_{n=1}^M C_{mn} = \sqrt{\frac{\pi}{g_m}} \frac{1 - \xi_m}{\lambda_M - \lambda_1} \frac{M - 1}{M}. \quad (23)$$

In the limit $M \rightarrow \infty$, the last fraction goes to 1, and we recover the continuum limit obtained in the main text.

$D_{\mathcal{P}}$ is defined as $1/\langle \tilde{w}_m \rangle$. To proceed, we introduce the length element and its relative fluctuation,

$$\delta \ell_m \equiv \sqrt{g_m} \delta \lambda = \langle \delta \ell_m \rangle (1 + \sigma_i) \quad , \quad \sigma_m \equiv \frac{\delta \ell_m - \langle \delta \ell_m \rangle}{\langle \delta \ell_m \rangle} = \frac{M \delta \ell_m}{\mathcal{L}} - 1 \quad , \quad (24)$$

where $\mathcal{L} = \sum_{m=1}^M \delta \ell_m = M \langle \delta \ell_m \rangle$. Then

$$\langle \tilde{w}_m \rangle = \frac{\sqrt{\pi}}{M} \left\langle \frac{1 - \xi_m}{\delta \ell_m} \right\rangle = \frac{\sqrt{\pi}}{\mathcal{L}} \left\langle \frac{1 - \xi_m}{1 + \sigma_m} \right\rangle \quad (25)$$

$$= \frac{\sqrt{\pi}}{\mathcal{L}} \sum_{a=0}^{\infty} (-)^a \langle (1 - \xi_m) \sigma_m^a \rangle \quad (26)$$

$$= \frac{\sqrt{\pi}}{\mathcal{L}} [1 - \langle \xi_m \rangle + \langle \sigma_m^2 \rangle + \langle \xi_m \sigma_m \rangle - \langle \xi_m \sigma_m^2 \rangle + \mathcal{O}((1 - \xi) \sigma^3)] \quad . \quad (27)$$

For a smooth curve, $\sigma_m^2 \ll 1$. Thus one can truncate at the σ_m^2 order,

$$D_{\mathcal{P}} = \frac{1}{\langle \tilde{w}_m \rangle} = \frac{\mathcal{L}}{\sqrt{\pi}} \left\langle \frac{1 - \xi_m}{1 + \sigma_m} \right\rangle^{-1} \simeq \frac{\mathcal{L}}{\sqrt{\pi}} (1 + \langle \xi_m \rangle - \langle \sigma_m^2 \rangle + \dots) \quad . \quad (28)$$

As discussed before, with increasing system size, $\langle \xi_m \rangle$ decreases, thus in the thermodynamic limit, the leading order correction should be $\langle \sigma_m^2 \rangle$.

Fig. 5 shows σ_m in the SSH model with three different system sizes, note that it is size independent. Numerical values of the expansion terms in Eq. 27 with $N = 50000$ unit cells are

$$\begin{array}{c|c|c|c} \langle \xi_m \rangle & \langle \sigma_m^2 \rangle & \langle \xi_m \sigma_m \rangle & \langle \xi_m \sigma_m^2 \rangle \\ \hline 0.0067 & 0.0018 & 0.00067 & 0.000066 \end{array} \quad . \quad (29)$$

Alternative definition of characteristic dimensionality

As discussed in the text, $1/\tilde{w}_m$ counts the number of random states in $\{|\Psi_n\rangle\}$ needed to represent $|\Psi_m\rangle$, and to remove the m dependence, there are two natural choices, $\langle 1/\tilde{w}_m \rangle$ and $1/\langle \tilde{w}_m \rangle$, where $\langle \dots \rangle = \sum_{m=1}^M (\dots)/M$. We have

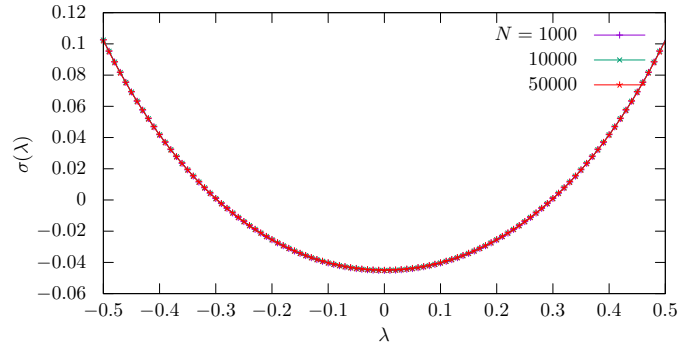


FIG. 5. σ correction in the SSH model with periodic boundary condition. Using 1000 ground states evenly sampled between $-0.5 < \lambda < 0.5$. Note that σ is size independent ($2N =$ number of lattice sites).

defined $D_{\mathcal{P}} = 1/\langle \tilde{w}_m \rangle$ in the text, but the second choice has its own merit, as it naturally evaluates to the geometric length. In the thermodynamic limit, one can ignore the edge correction ξ (see Fig. 4), then

$$D_{alt} \equiv \langle \frac{1}{\tilde{w}_m} \rangle = \frac{1}{M} \sum_{m=1}^M \frac{1}{\tilde{w}_m} \xrightarrow{\xi_m=0} \frac{1}{\sqrt{\pi}} \sum_{m=1}^M \sqrt{g_m} \delta\lambda = \frac{\mathcal{L}}{\sqrt{\pi}}. \quad (30)$$